A Low-cost, 20-DOF Anthropomorphic Robotic Hand: Design, Actuation and Modeling

Author Names Omitted for Anonymous Review. Paper-ID [162]

Abstract—In order to effectively develop the control methods of an anthropomorphic robotic hand, it is important for researchers to have fast and easy access to modify any design parameters. To this end, we detail the process of designing a 20 degrees of freedom, cable-driven, anthropomorphic robotic hand. The prototyping process makes the most of 3D printing technology, and takes important factors such as maintainability and modification into consideration. Skin pads and finger segments of the robotic hand can all be quickly assembled with other components through reliable, structural coupling. And each modular finger can be individual modified with little effort. We also adopt a custom-designed physics engine to model the robotic hand in order to efficiently compute the kinematic configuration. Good performance of tactile sensing, force behaviors, and actuation speed are observed in experiments. Overall, we show our anthropomorphic robotic hand to be cost-effective and flexible to design and control requirements.

Fig. 1: The 3D-printed 20-DOF anthropomorphic robotic hand.

I. INTRODUCTION

The benefits of investigating anthropomorphic robotic hands have been widely acknowledged, and some of them have been effectively demonstrated, such as the highly biomimetic robotic hand designed for understanding the human hand [4], lightweight prosthetic hands with improved functionalities [8, 14], and many other anthropomorphic robotic hands developed for investigating dexterous manipulation [1, 2, 3, 7, 9, 10, 12, 13, 15, 17].

However, it is also widely accepted that the cost of time and grant funding on developing a research-oriented, custom-designed anthropomorphic robotic hand is often prohibitive. The control of a robotic hand can be affected by many factors, such as the finger length, the range of motion (ROM) of the joints, the weight of the robotic hand, or transmission types. Many researches had to shape their control goals by the limits of commercially available anthropomorphic robotic hands due to the fact that even the slightest modification on those off-the-shelf robotic hands could easily result in months of waiting.

For those researches focusing on the hardware aspects of anthropomorphic robotic hands, it is also challenging to modify the design or improve the functionalities of an existing system in a short period of time. This is because each of the design iterations needs to go through the validation of physical tests before any useful information can be collected for planning any improvement. Therefore simulation as a promising tool to help evaluating the performance of robotic hands has been adopted to speed up the design process [11].

Many anthropomorphic robotic hands were designed to be cable-driven [1, 2, 7, 9, 10, 13, 16, 17]. On the one hand, it is intuitive to mimic the muscle-tendon mechanism of the human hand with cables and wires; on the other hand, this is because

the cable-driven robotic hand system possesses several advantages including back-drivable, backlash-free, light weight, and the flexibility for the robotic hand to choose between being fully actuated and being under-actuated depending on needs of different application. So far numerous efforts have been put into the development of simulation software, however, none of the existing physics engines could handle the level of the complexities posed by a 20 degrees of freedom (DOFs), cable-driven anthropomorphic robotic hand.

In this paper, we take an alternative approach to the question of how the anthropomorphic robotic hand can be designed such that the fabrication of the robotic hand is fast, the cost of the modification and maintenance is cheap, and the control of the robotic hand is feasible by presenting the design, actuation, and modeling of a 20-DOF anthropomorphic robotic hand (as shown in Figure 1). Our proposed method combines adaptive design, rapid prototyping, and modeling with a custom-designed software [5]. The resulted anthropomorphic robotic hand is composed of 31 parts in comparison to other existing robotic hands using hundreds of parts, and can be 3D-printed in 20 hours and fully assembled in 4 hours. Its size, DOFs, ROM, and actuation type can all be adjusted/changed with little effort or modification.

In the following sections, the innovative design methods of the robotic hand are detailed, the actuation system is described, and then the modeling of the robotic hand system is established to demonstrate how our custom modeling software could help to speed up the control. At the end a fully assembled robotic hand system is prepared for our future work.
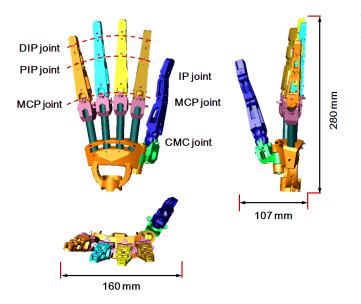
Fig. 2: 3D model of the anthropomorphic robotic hand.

TABLE I: The joint motion limits of the anthropomorphic robotic hand

Finger	Joint	Minimum	Maximum
Index,	MCP	20° extension	90° flexion
Middle,		30° abduction	30° adduction
Ring,	PIP	0° extension	90° flexion
& Little	DIP	0° extension	90° flexion
Thumb	CMC	40° extension	90° flexion
		40° abduction	40° adduction
	MCP	0° extension	80° flexion
	IP	20° extension	90° flexion

II. DEVELOPMENT OF THE ANTHROPOMORPHIC ROBOTIC HAND

Although the anatomy of the human hand provides detailed sources of static models, such as joint structure, tendons routing, and layered skin, how to organically incorporate state-of-the-art engineering advances into a fully functional robotic hand system is what we want to achieve in this paper. This section describes the mechanical design and prototyping process of our robotic hand.

As shown in Figure 2, Our proposed robotic hand is composed of four articulated fingers and one opposable thumb. In order to accurately match the size and shape of the human hand, a laser-scan model of a human left hand (Stratasys Corp., Eden Prairie, MN) was used to decide the length of each finger and the location of joints.

There are three joints in each finger of the human hand: namely, the metacarpophalangeal (MCP), proximal interphalangeal (PIP), and distal interphalangeal (DIP). Each DIP and PIP joint possesses one DOF. The MCP joint has two DOFs: one to achieve flexion-extension and another to realize abduction-adduction finger motion. The three joints of the thumb are the carpometacarpal (CMC), metacarpophalangeal (MCP), and interphalangeal (IP) joints. Its IP and MCP joint were designed to possess one rotation DOF in the flexion-extension direction. In contrast with other fingers MCP joints, the CMC joint of the thumb has two DOFs with two non-intersecting, orthogonal axes. Table I lists the ROM of our proposed robotic hand.

A. 3D-printed Lego-style, modular finger design

As previously mentioned, one of the major barriers that prevents researchers from adding modification to any existing anthropomorphic robotic hands is that the cost of time and grand funding. However this cost can be side stepped through
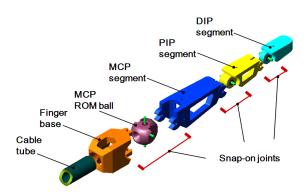

Fig. 3: Components of each finger unit.

the innovation of rapid prototyping technologies. As shown in Figure 3, each segment of a finger is 3D printed by the Dimension BST 768 (Stratasys Corp., Eden Prairie, MN). The resolution of the 3D printed parts is 0.025mm, and it takes only one hour to print all the components of an entire finger. Additionally the strength of the ABS plastic is sufficient to resist the induced stress of cables.

Fig. 4: Two examples of assembling a Snap-On joint. *Top row: assembling a DIP hinge joint.* Bottom row: *assembling a MCP ROM-ball on to the finger base*

One of the important factors we believe that makes LEGO toy popular is because it allows players to inspiringly prototype their design ideas via a number of interlocking plastic bricks within a short period time. Following the same principle, our proposed robotic hand was designed to be modular and adaptable. The joint connection between two finger segments was formed by one LEGO-style Snap-On joint. As shown in

Figure 3, there are three Snap-On joints in one finger. The interlocking mechanism of the Snap-On joint is composed of a 3D printed C-shaped clip on one side of the joint and a steel shaft passing through the center of the other side of the joint. After snapping into the clip, the steel shaft can be secured by the friction engagement, and a Snap-On joint is thus formed (as shown in Figure 4).

The ROM of a joint is limited by the mechanical constraints between adjacent finger segments in extreme postures and can be modified in CAD model without affecting other sites of the part. For instance, by snapping on a new MCP ROM-ball with different mechanical constraints, the ROM of abduction/adduction can vary from 20 degrees to 40 degrees easily.

In addition to simplifying the robotic hand design, the Snap-On mechanism can also help to ease the burden on assembly: by replacing a set of finger segments with shorter ones, a smaller hand will be reformed in minutes.

B. Adaptable tendon routing

The tendon routing plays an important role in control of anthropomorphic robotic hands. As shown Figure 5(a), our proposed robotic hand used four pairs of antagonistic tendons to control each of its 4-DOF fingers. The tendons are made of 0.46 mm Spectra® fiber (AlliedSignal, Morristown, NJ). The fiber was chosen because of its strength (200N breaking strength), high stiffness, flexibility, and its ability to slide smoothly through the cable tube. Compared to other types of transmission, such as linkages, gears, and belts, choosing cable-driven system enables the anthropomorphic robotic hand to quickly switch between being fully actuated and being under-actuated with little modification as shown in Figure 5. This in return broadens the application of the anthropomorphic robotic hand ranging from dexterous manipulation research to practical prosthetics.

Although changing the tendon routing is a good way to explore the potentials of an anthropomorphic robotic hand, it is also the most time-consuming process during the assembly (e.g., 90% of the total time in our case). How to efficiently optimize the cable routing and paths so that each of the finger joints can be controlled properly plays an important role in our proposed robotic hand design.

Before rushing to prototype/modify the robotic hand, our custom modeling software provided us an unique platform to evaluate our design ideas. For instance, the STL files generated for 3D printing can be directly loaded into the software for detecting mechanical conflicts.

C. Tactile sensing of the robotic hand

The tactile sensing field of the hand is composed of 16 independent skin pads, each of which consists of three layers as shown in Figure 6. From the skin's surface (top) to the skeleton (bottom), they are: Velcro embedded in artificial skin (silicon rubber), a tactile sensing element (sensel), and a 3D printed frame.

The layer of artificial skin is made of silicon rubber (Plat-Sil ® 71 Series RTV, Polytek Development Corp., Easton, PA)
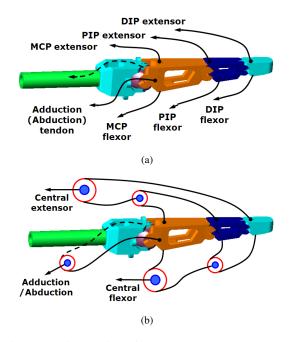

(a)

(b)

Fig. 5: Schematic drawing of two possible cable routing types. *(a)* A 4-DOF finger with four pairs of antagonistic cables (*Note:* cables originated from the DIP and PIP finger segments were passing through the center of the cable tubes in the real robotic hand, for better illustration, their routings are drawn explicitly). *(b)* A 3-DOF under-actuated finger with pulley systems.
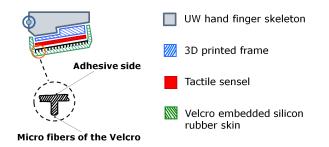

Fig. 6: Schematic drawing of artificial skin's multi-layered structure (Note: differently colored regions are not in proportion to the real distributions of those layers.)

with high shear strength. Its shape is cast by a set of 3D printed molds (see Figure 7) which forms a tapered shape resembling the pad of the human's fingertip. The fingerprint on its contacting surface can be custom designed to possess different surface textures which will affect its sensing performance. The hydrophobic property of the silicon rubber provides the artificial skin with beneficial properties such as easy-clean, water and oil resistant, and anti-smudge coatings but this also prohibits the silicon from sticking to any adhesive. This poses a big challenge when bonding it with neighboring layers. This problem has been innovatively solved by making the most of Velcro as follows: Before the silicon rubber becomes fully cured, a slice of Velcro (loop side) is embedded into the
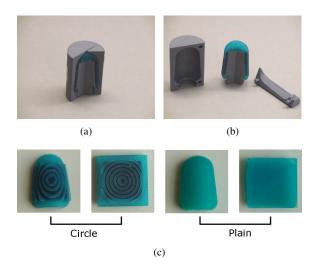
(a)   (b)

(c)

Fig. 7: The prototyping process of the artificial skin. *Top row:* Components of the molds used for prototyping the fingertip's skin. *Bottom row:* Skin pads with different textures on two types of skin shapes.

skeletal side of the skin layer. After the curing process, the Velcro is securely bonded due to the strong interaction between a large number of micro fibers and their surrounding silicon rubber. The whole skin layer can then be easily adhered to the sensel through the adhesive surface of the Velcro. The total thickness of this top most layer through to the Velcro is about 2 mm. To achieve optimal performance (and durability) of the silicon rubber a vacuum chamber is used to remove any air bubbles from the silicon mixture before curing.
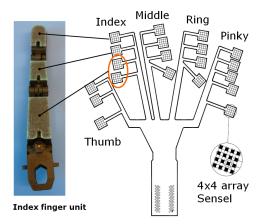

Fig. 8: The configuration of the tactile sensor as the 2nd layer of the artificial skin.

The second layer is formed by a 4×4 (20×20 mm in dimension) sensel array from an off-the-shelf five finger Grip ^{TM} system (Tekscan Inc., South Boston, MA) for identifying the location and magnitude of pressure points on the hand (see Figure 8). The Grip ^{TM} system made in this way has paper-thin flexibility (0.1 mm in thickness). After binding with the Velcro's adhesive surface, the sensor layer is carefully wrapped

onto the 3D printed frame and attached with an adhesive (3M 77 spray adhesive). The sensel is more strongly bound to the printed frame than the Velcro; the bonding on either side of the sensel prevents slippage.

The third layer is a 3D-printed frame and works as a skeletal component of the whole structure, and determines the basic shape and contour of the artificial skin. Its outer surface is bonded with the tactile sensel, while its other side is structurally coupled with the finger's skeleton via the opening on each segment of the fingers. The resulted skin pad can be easily put on and off making maintenance of the artificial skin possible – worn silicon rubber can easily be snapped off and replaced with a new one. Because the Velcro's bonding with the sensel is weaker than the sensel's bond to the frame the sensel remains attached to the frame during replacement.

This skin design can potentially improve manipulation performance by providing tactile sensing and more reliable grasping forces, and its performance will be evaluated in the experimental section.

D. Actuation system

As shown in Figure 9 the actuation system consists of two major components: pneumatic control unit, and robotic hand's actuation unit.
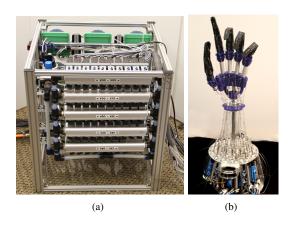

(a)   (b)

Fig. 9: The actuation system of the robotic hand. *Left:* the pneumatic control unit. *Right:* Fully assembled actuation unit.

The actuation unit contains 36 of the M9 Airpel cylinders (Airpot Corp., CT) for finger tendons, and 4 of the M16 Airpel cylinders for wrist tendons (also used for finger actuation in this work). Double-acting cylinders were selected for complete control over the actuation force in both directions (although this feature is not yet utilized). The fully assembled actuation unit forms the base of the hand and weighs 660 grams. It can sustain about 75 N from each air cylinder with a safety factor of 3. When attached to a robot arm, most of this mass is near the base (elbow), thus won't cause mechanical conflicts during manipulation tasks.

Due to the page limit, interested reader can find detailed specifications from our previous work [6].

III. MODELING OF THE ROBOTIC HAND

The variable moment arms of our proposed robotic hand closely mimic its human counter-part, and provide us an unique opportunity to investigate dexterous manipulations tasks. However, it also poses a series of challenges to the robotic hand control. Together with the information of the tendon excursion, knowing accurate moment arms at each joint of the finger can allow us to easily compute the kinematic configuration including joint angles and velocities for the corresponding finger.
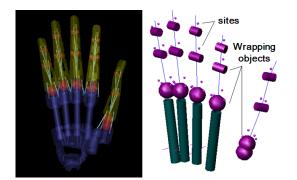

Fig. 10: Modeling of the robotic hand. *Left:* Kinematic model of the robotic hand visualized in OpenGL. *Right:* The model of the tendon paths.

Instead of complicating the mechanical structure of our robotic hand by adding multiple joint sensors, we chose to construct a kinematic model of the hand and its tendon paths in order to estimate the finger status(as shown in Figure 10) This was done by taking the numeric data from the CAD file used to 3D-print the robotic hand, and importing it in an XML file that is then read by our modeling software. Our softwareis a fully featured new physics engine, with a number of unique capabilities including simulation of cable actuation via complex surfaces. In this paper we only use the kinematic modeling features of the engine, as well as the built-in OpenGL visualization.
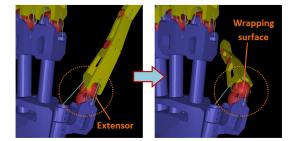

Fig. 11: The thumb extensor wrapping at the CMC joint during the flexion motion.

The skeletal modeling approach is standard: the system configuration is expressed in joint space, and forward kinematics are used at each time step to compute the global positions and orientations of the body segments along with any objects attached to them. Tendon modeling is less common and so we describe our approach in more detail. The path of the cable is determined by a sequence of routing points (defined as sites) as well as geometric wrapping objects which can be spheres or cylinders (as shown in Figure 10). As shown in Figure 11 the software computes the shortest path that passes through all sites defined for a given tendon, and does not penetrate any of the wrapping objects (i.e. the tendon wraps smoothly over the curved surfaces). The latter computation is based on the Obstacle Set method previously developed in biomechanics.

Let $\mathbf{q}$ denote the vector of joint angles, and $\mathbf{s}_1(\mathbf{q}), \cdots, \mathbf{s}_N(\mathbf{q})$ denote the 3D positions (in global coordinates) of the routing points for a given cable. These positions are computed using forward kinematics at each time step. Then the cable length is

$$L(\mathbf{q}) = \sum_{n=1}^{N-1} \left((\mathbf{s}_{n+1}(\mathbf{q}) - \mathbf{s}_n(\mathbf{q}))^T (\mathbf{s}_{n+1}(\mathbf{q}) - \mathbf{s}_n(\mathbf{q})) \right)^{1/2}$$

The terms being summed are just the Euclidean vector norms $\|\mathbf{s}_{n+1} - \mathbf{s}_n\|$, however we have written them explicitly to clarify the derivation of moment arms below. When the cable path encounters a wrapping object, additional sites are dynamically created at points where the cable path is tangent to the wrapping surface. These sites are also taken into account in the computation of lengths and moment arms.

Moment arms are often defined using geometric intuitions – which work in simple cases but are difficult to implement in general-purpose software that must handle arbitrary spatial arrangements. Instead we use the more general mathematical definition of moment arm, which is the gradient of the cable length with respect to the joint angles. Using the chain rule, the vector of moment arms for our cable is

$$\frac{\partial L(\mathbf{q})}{\partial \mathbf{q}} = \sum_{n=1}^{N-1} \left(\frac{\partial \mathbf{s}_{n+1}(\mathbf{q})}{\partial \mathbf{q}} - \frac{\partial \mathbf{s}_n(\mathbf{q})}{\partial \mathbf{q}} \right)^T \frac{\mathbf{s}_{n+1}(\mathbf{q}) - \mathbf{s}_n(\mathbf{q})}{\|\mathbf{s}_{n+1}(\mathbf{q}) - \mathbf{s}_n(\mathbf{q})\|}$$

This expression can be evaluated once the site Jacobians $\partial \mathbf{s}/\partial \mathbf{q}$ are known. Our software automatically computes all Jacobians, and so the computation of moment arms involves very little overhead.

Numerical values for the moment arms change with hand configuration in a complex way, and are automatically recomputed at each time step. Moment arms are useful for computing the cable velocities given the joint velocities:

$$\dot{L} = \frac{\partial L(\mathbf{q})}{\partial \mathbf{q}} \dot{\mathbf{q}}$$

Examples of measured moment arms of the robotic hand's index finger are shown in Figure 12.

IV. PERFORMANCE EVALUATION OF THE ROBOTIC HAND

In this section, we conducted a series of experiments to test the performance of the tactile sensing, compliance, and speed of our proposed robotic hand. Preliminary results are reported.
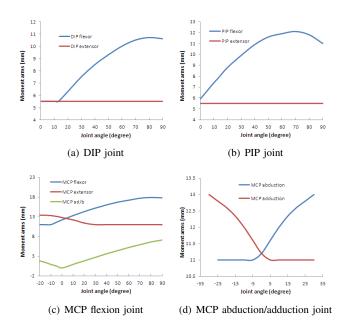
(a) DIP joint

(b) PIP joint

(c) MCP flexion joint

(d) MCP abduction/adduction joint

Fig. 12: Moment arms at different joints of the index finger of the robotic hand. *(a)* Moment arms at the DIP joint. *(b)* Moment arms at the PIP joint. *(c)* Moment arms at the MCP flexion joint. *(d)* Moment arms at the MCP abduction/adduction joint.(*Note:* Flexion and abduction motions have positive angles, flexion; extension and adduction motions have negative angles.)

A. The performance of the tactile sensing

As showin in Figure 13, we designed an experiment to simulate a pinch where small contact areas are often limited to the fingertips. For this physical simulation we used a 3-DOF Phantom Premium 1.5A (SensAble Technologies, Inc., Wilmington, MA), with a special end-effector (the probe, 10 mm in diameter), to replicate an object impinging on the skin's surface. This mimics the situation of holding an object between the thumb and index fingertips, where the thumb force is produced by the Phantom robot and the object is the probe.

The length of the probe was decided in such a way that the center of the contacting point on the probe (as labeled by red round dots in Figure 13) could match the acting point of the Phantom's end-effector. The size of the spherical probe was chosen based on a contacting surface test: A piece of planar glass was used to push against the human fingertip firmly, through the transparent glass the average diameter of the deformed area on the fingertip was then used as the diameter of spherical probe.

At the beginning of each trial, the probe was manually placed onto the spot close to the center of the skin pad fixed onto the sensor jig. And then the displacement, velocity, and forces of the probe at the contacting point were recorded at 1000Hz. The average sampling rate of the force sensor used in this work is 20Hz. Once the probe was positioned properly, 3.5 N of normal force in Y-direction, and a 1 N of tangential force in Z-direction (both in the Phantom frame)
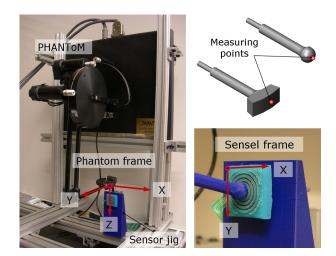

Fig. 13: *Left:* Experimental setup. *Top right:* Two different shapes of the probes: the sphere (10 mm in diameter) and the curved surface (47 mm in radius). *Bottom right:* Initial test position. *Note:* the difference between the Phantom and sensel frames.

were simultaneously commanded onto the surface of the skin pad through the probe. While keeping the tangential force consistent, the normal force was controlled to gradually decrease with a constant rate of 0.3N/s. Each trial ended at the moment when the probe eventually slipped off from the skin pad.

Raw data from the sensel were used to estimate the displacement of pressure center along vertical direction by using the following equation:

$$D_{centroid} = \frac{\sum f_i y_i}{\sum f_i}$$

The force reading from the sensel at the center of pressure, with respect to the sensel's frame is calculated as,

$$F_{centroid} = \frac{\sum f_i y_i}{\sum y_i}$$

Figure 14 shows the results from the case of a spherical probe and hexahedral skin pad (with circled texture). The shaded areas in Figure 14 (a) and (c) represent initial probe adjustment before trial onset. The contacting force was measured by the skin pad (see Figure 14 (a)). Onset of each trial is defined by the peak of the sensel's force. The calculated and actual displacements of the pressure center are compared in Figure 14 (c). It is clear that the estimated center of pressure agrees quite well with the recorded data. And the trend of slip could also be observed.

B. The force behaviors and speed of the robotic hand

In order to investigate the characteristics of the force and compliance of the actuation system, we conducted experiments using a Shadow hand in our previous work [6]. In this paper, we conducted the same experiments on our proposed robotic hand and compare its performance with the Shadow hand in Table II. An external force of 2 grams at the index finger
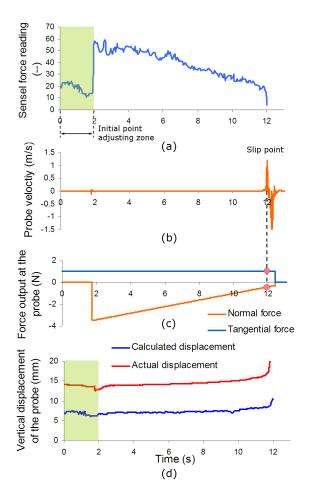
Fig. 14: Output of the tactile sensing. *(a)* Force reading from the sensel. *(b)* The probe velocity measured from the Phantom's end-effector. *(c)* The output of normal and tangential forces from the Phantom robot. *(d)* Comparison of the calculated (in sensel frame) and measured (in Phantom frame) displacement of the probe along vertical direction.

TABLE II: Comparison of characteristic force behaviors

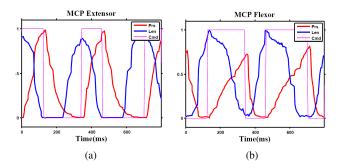| Specifications on force behaviors	Our proposed robotic hand	The Shadow hand
Minimum actuation force at finger tip to move MCP joint(vertical actuator, at atm pressure)	2.0 g	4.0 g
Minimum actuation force at finger tip to move MCP joint(vertical actuator, at min slack correction pressure)	8.0 g	6.0 g
Maximum flexion force at index finger tip	705 g	300.5 g
Maximum extension force at index finger tip	700 g	439.4 g

Fig. 15: Full finger motion at 3 Hz. *Left\Right:* Response of the valve pressure (prs) and length sensor (len) of the MCP extensor\flexor with respect to the command signal.
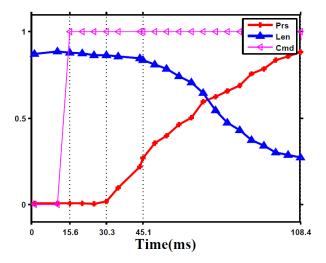

Fig. 16: Time stamps. *From left to right:* T1 – Event Trigger, command written to the pneumatic value, T2 – Pressure wave arrival, T3 – Index finger MCP movement detected.

tip was enough to flex the MCP joint thus confirming the exceptional compliance of our fully actuated robotic hand. During the test of the maximum fingertip forces, all the index fingers of the two robotic hands were commanded to be fully extended, the moment arm of our proposed robotic hand is 13 mm (104 mm finger length) compared to Shadow hand's 10 mm moment arm (96 mm finger length), but produced over doubled forces in both flexion and extension directions.

The actuation system we developed was mainly prepared for the tendon-driven hands and performing dexterous hand manipulation experiments. Any dexterous hand manipulation demands agility and responsiveness from its actuation hardware. The speed capabilities of our robotic hand were evaluated using a simple open loop bang-bang control strategy over the index finger. The goal was to achieve full stroke movements (joint limit to joint limit) at maximum frequency. Control switching frequency was gradually increased until finger started making incomplete strokes, i.e. reversed before

hitting the joint limits. Using this simple strategy, a frequency of about $3Hz$ was achieved for a full finger motion (from fully extended to fully flexed for all the three joints) as shown in Figure 15 and 16. We are working towards a more principled way to further improve actuation speed by carefully modelling valve and pneumatics of our system. A video of the robotic hand in motion can be found from here.

C. The cost of the robotic hand

The cost of our proposed robotic hand itself is very low – approximately \$100 for all materials. Of course this does not include the tactile sensing (\$300) and actuation system. However, a ShadowHand robot with similar mechanical capabilities and also without actuation costs around \$60,000. Thus the proposed design offers a dramatic reduction in cost, as well as time required to manufacture and test a modified version of the system when needed.

A notable advantage of having an inexpensive hand (and instead investing in the actuation system) is that only the hand will typically interact with the environment. Thus any damage is likely to occur in parts that are inexpensive to replace. The modular design of the robotic hand and its tactile sensing can further reduce the cost as well.

V. Conclusion and future work

We have described the method of designing and modelling of a 20-DOF anthropomorphic robotic hand. Our proposed robotic hand has 31 components, and can be manufactured in 24 hours. Important parameters such as finger length, DOF, and ROM of the robotic hand can all be individually changed with little effort or modification. Skin pads for tactile sensing were also developed. For evaluating design ideas and speeding up our design cycle, we used our custom modeling software to establish the kinematic model of the robotic hand. Experimental results on tactile sensing, force behaviors and actuation speed suggested that our robotic hand has comparable performance to the ShadowHand robot, but requires only a fraction of the latter's cost. Our proposed design has the potential to become an important tool for assisting robotic hand researchers to cost-effectively and efficiently investigate different control methods.

In future work, besides using model based estimation for computing the kinematic configuration, we will implement joint sensors to our robotic hand and apply optimal control techniques to explore different manipulation tasks.

References

[1] V. Bundhoo and E.J. Park. Design of an artificial muscle actuated finger towards biomimetic prosthetic hands. In *12th International Conference on Advanced Robotics, 2005. ICAR '05. Proceedings.,*, pages 368 –375, July 2005.

[2] M. C. Carrozza, G. Cappiello, S. Micera, B. B. Edin, L. Beccai, and C. Cipriani. Design of a cybernetic hand for perception and action. *Biol. Cybern.*, 95(6):629–644, 2006. ISSN 0340-1200.

[3] Louis-Alexis Allen Demers and Clement Gosselin. Kinematic design of a planar and spherical mechanism for the abduction of the fingers of an anthropomorphic robotic hand. In *2011 IEEE International Conference on Robotics and Automation (ICRA),*, pages 5350 –5356, May 2011.

[4] A. D. Deshpande, Z. Xu, M. J. V. Weghe, B. H. Brown, J. Ko, L. Y. Chang, D. D. Wilkinson, S. M. Bidic, and Y. Matsuoka. Mechanisms of the Anatomically Correct Testbed Hand. *IEEE/ASME Transactions on Mechatronics*, (99):1–13, 2011.

[5] Author Names Omitted for Anonymous Review. Mujoco: a physics engine for model-based control. In *IEEE/RSJ International Conference on Intelligent Robots and Systems*, 2012.

[6] Author Names Omitted for Anonymous Review. Fast, strong and compliant pneumatic actuation for dexterous tendon-driven hands. In *2013 IEEE International Conference on Robotics and Automation* (to appear,, 2013.

[7] M. Grebenstein, M. Chalon, G. Hirzinger, and R. Siegwart. Antagonistically driven finger design for the anthropomorphic DLR Hand Arm System. In *2010 10th IEEE-RAS International Conference on Humanoid Robots (Humanoids),*, pages 609 –616, Dec. 2010.

[8] Peter J. Kyberd, Colin Light, Paul H. Chappell, Jim M. Nightingale, Dave Whatley, and Mervyn Evans. The design of anthropomorphic prosthetic hands: A study of the southampton hand. *Robotica*, 19(6):593–600, 2001. ISSN 0263-5747.

[9] F. Lotti, P. Tiezzi, G. Vassura, L. Biagiotti, G. Palli, and C. Melchiorri. Development of UB Hand 3: Early results. In *Proceedings of the 2005 IEEE International Conference on Robotics and Automation*, pages 4488–4493, April 2005.

[10] C.S. Lovchik and M.A. Diftler. The Robonaut hand: a dexterous robot hand for space. In *Proceedings of the 1999 IEEE International Conference on Robotics and Automation.*, volume 2, pages 907–912, 1999.

[11] A.T. Miller and P.K. Allen. Graspit! a versatile simulator for robotic grasping. *IEEE Robotics Automation Magazine*, 11(4):110 – 122, 2004.

[12] Tetsuya Mouri, Haruhisa Kawasaki, Yoshikawa Keisuke, Jun Takai, and Satoshi Ito. Anthropomorphic robot hand: Gifu hand III. In *Proc. Int. Conf. ICCAS*, 2002.

[13] F. Rothling, R. Haschke, J.J. Steil, and H. Ritter. Platform portable anthropomorphic grasping with the bielefeld 20-DOF Shadow and 9-DOF TUM hand. In *IEEE/RSJ International Conference on Intelligent Robots and Systems*, 2007.

[14] Touch Bionics Inc. www.touchbionics.com, 2009.

[15] Jun Ueda, Y. Ishida, M. Kondo, and T. Ogasawara. Development of the NAIST-Hand with vision-based tactile fingertip sensor. 2005.

[16] Zhe Xu, Vikash Kumar, Yoky Matsuoka, and Emanuel Todorov. Design of an anthropomorphic robotic finger system with biomimetic artificial joints. In *2012 4th IEEE RAS EMBS International Conference on Biomedical Robotics and Biomechatronics (BioRob)*, pages 568 –574, june 2012.

[17] I. Yamano and T. Maeno. Five-fingered robot hand using ultrasonic motors and elastic elements. In *Proceedings of the 2005 IEEE International Conference on Robotics and Automation.*, pages 2673–2678, April 2005.